Journal of Urban and Environmental Engineering
E-ISSN: 1982-3932
celso@ct.ufpb.br
Universidade Federal da Paraíba
Brasil

de S. I. Gonçalves, Julio Cesar; F. Giorgetti, Marcius
MATHEMATICAL MODEL FOR THE SIMULATION OF WATER QUALITY IN RIVERS USING THE VENSIM PLE® SOFTWARE
Journal of Urban and Environmental Engineering, vol. 7, núm. 1, -, 2013, pp. 48-63
Universidade Federal da Paraíba
Paraíba, Brasil

Journal of Urban and Environmental Engineering, v.7, n.1, p.48-63

ISSN 1982-3932
doi: 10.4090/juee.2013.v7n1.048063

Journal of Urban and Environmental Engineering

www.journal-uee.org

MATHEMATICAL MODEL FOR THE SIMULATION OF WATER QUALITY IN RIVERS USING THE VENSIM PLE® SOFTWARE

Julio Cesar de S. I. Gonçalves[1*] and Marcius F. Giorgetti[2]

[1]*Department of Environmental Engineering, Federal University of Triângulo Mineiro, Brazil*
[2]*School of Engineering of São Carlos, University of São Paulo, Brazil*

Received 25 January 2013; received in revised form 20 March 2013; accepted 04 April 2013

Abstract: Mathematical modeling of water quality in rivers is an important tool for the planning and management of water resources. Nevertheless, the available models frequently show structural and functional limitations. With the objective of reducing these drawbacks, a new model has been developed to simulate water quality in rivers under unsteady conditions; this model runs on the Vensim PLE® software and can also be operated for steady-state conditions. The following eighteen water quality variables can be simulated: DO, BOD_c, organic nitrogen (N_o), ammonia nitrogen (N_a), nitrite (N_i), nitrate (N_n), organic and inorganic phosphorus (F_o and F_i, respectively), inorganic solids (Si), phytoplankton (F), zooplankton (Z), bottom algae (A), detritus (D), total coliforms (TC), alkalinity (Al.), total inorganic carbon (TIC), pH, and temperature (T). Methane as well as nitrogen and phosphorus compounds that are present in the aerobic and anaerobic layers of the sediment can also be simulated. Several scenarios were generated for computational simulations produced using the new model by using the QUAL2K program, and, when possible, analytical solutions. The results obtained using the new model strongly supported the results from the QUAL family and analytical solutions.

Keywords: Modeling; water quality; Vensim PLE; rivers

* Correspondence to: Julio Cesar de S. I. Gonçalves, Tel.: +55 34 3318 5600.
E-mail: julio@icte.uftm.edu.br

INTRODUCTION

In the past few decades, rivers have become the main recipients of wastewater that is generated from municipal and industrial sources with little to no treatment prior to discharge is common practice in many developing countries (Ghosh & McBean, 1998; Zhang *et al.*, 2012). River pollution is one of the most serious water resources problems of the present day. These problems for various river systems have been reported frequently (Drolc & Koncan, 1996; Liu *et al.*, 2005; Gonçalves *et al.*, 2011).

Water quality modeling is increasingly recognized as a useful tool for acquiring valuable information for optimal water quality management. In recent years, water quality models have been widely applied such as QUAL2E and QUAL2K (Ghosh & McBean, 1998; Park & Lee, 2002; Sardinha *et al.*, 2008; Salvai & Bezdan, 2008; Zhang *et al.et al.*, 2012). QUAL2K is a modern version of QUAL2E (Brown & Barnwell, 1987). They were developed by the U. S. Environmental Protection Agency, the EPA, to evaluate the self-depuration capacity of rivers in the United States that receive treated sewage of urban origin.

The QUAL2E model has limitations, as it was created specifically to analyze the effects of steady sources of pollution under American standards. Simulating a stream that is subjected to unsteady sources of pollutants is very difficult with the QUAL2E model.

Steady-state modeling is inadequate if the objective is, for instance, to describe water quality in a stream that has been subjected to accidental spills. These may occur if there is a rupture in a storage tank, or in a pumping line at a sewage treatment station. In such cases, a large load of organic matter can be quickly dumped into a stream, causing an intense deterioration of the aquatic environment.

Another limitation found in the majority of water quality models, including the QUAL2K, is that it is difficulty (or even impossible) for a user to modify its internal structure. The model includes empirical relationships or equations that reflect the specific conditions for which the model was first developed. Consequently, the user cannot introduce relationships or equations that better describe the case under analysis.

On the other hand, it is impossible when using some models, but not QUAL2K, to assign different values for the kinetic coefficients for different stretches along the length of a river. This becomes a serious limitation when effluents with distinct rates of biodegradation are discharged into different points of the stream. Consider, for instance, the case of a discharge of effluents from a domestic sewage treatment plant and from a pulp and paper mill treatment station into a river. The adoption of a single coefficient of biodegradation for water quality modeling in such a river would underestimate the actual impact and reduce the modeling capacity.

Given the relatively high frequency of accidental spills, the diversity of the effluents being discharged into a stream, and the need for mathematical models to be easy to understand and implement, a new modeling system that overcomes the limitations described above is needed. To accomplish this, the authors used the Vensim PLE® software, developed by Ventana Systems, Inc.

The potential of the Vensim PLE® software for modeling unsteady water quality problems was established after a thorough comparison of the software to the analytical solutions for a hypothetical scenario of a short duration spill, in cases where an analytical solution existed. Other hypothetical scenarios were built to demonstrate the tools of the Vensim PLE® software that facilitate building models for an unsteady-state regime.

THE VENSIM PLE® SOFTWARE

The Vensim PLE® software, adopted for this work, is made available at the website of Ventana Systems, Inc. and can be downloaded free of charge for academic use. Models built using this software are much simpler than those created with typical programming languages.

Vensim PLE® models are built as cause diagrams, or diagrams of stocks and rates. Stocks are represented by rectangles (box variables), and rates are represented by arrows on double solid lines pointing into a box (rate in) or out of a box (rate out). The arrows have valves (two opposing small triangles) that can control the rates into and out of a box. Clouds at the extremes represent sources or sinks of a quantity being transported to or from a box (**Fig. 1**).

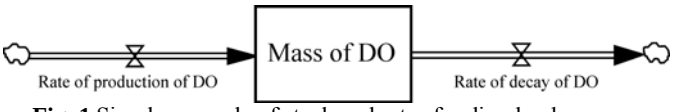

Fig. 1 Simple example of stock and rates for dissolved oxygen.

Stocks are also called integrals, state variables, or lungs; rates are time derivatives. In **Fig. 1**, the mass of DO at time t is equal the mass of DO at t = t_0 plus the integral of the rate of production minus the rate of decay over t from t_0 to t. The **Eq. (1)** is as follows:

$$M_{O_2}(t) = M_{O_2}(t_0) + \int_{t_0}^{t} [T_p - T_d]\, dt \qquad (1)$$

where M_{O_2} : mass of DO (M); T_p: rate of production of DO (M/T); and T_d: rate of decay of DO (M/T).

The Vensim PLE® software offers two alternatives for numerical integration, namely Euler's method and the fourth order Runge-Kutta method (RK4).

BUILDING THE MODEL FOR A WATER COLUMN

The development of a water quality model involves building two sub-systems, one for the hydraulics of the water body (balance of volume), and another describing causes for the changes in concentration of the water quality variables, namely, the chemical, physical and biological processes, and the transport mechanisms represented by advection, diffusion and dispersion.

When building a model, a river channel is divided into control volumes (CV) of length Δx, each one comprising two sub-systems as described in the preceding paragraph.

To balance volume at steady-state conditions, the flow rate out of the CV equals the sum of the flow rates into the CV (flow rate from the upstream CV plus flow rate from sources of pollution) minus the flow rate of the water sinks (pumping stations). This equation is:

$$Q_i = Q_{i-1} + Q_{fp,i} - Q_{Cs,i} \quad (2)$$

where Q_i: flow rate out of CV i and flow rate into downstream CV i+1 (L^3/T); Q_{i-1}: flow rate into CV i and flow rate out of upstream CV i+1 (L^3/T); $Q_{fp,i}$: flow rate from sources of pollution into CV i (L^3/T); and $Q_{cs,i}$: flow rate of water pumped out of i (L^3/T).

The term $Q_{fp,i}$ is also used to represent the flow rate from a tributary of the river that can be modeled if necessary.

The differential equation resulting from the balance of volume used for modeling with Vensim PLE® is shown below:

$$\frac{dV}{dt} = Q_i + Q_{i-1} + Q_{fp,i} - Q_{Cs,i} \quad (3)$$

The combination of **Eqs (2)** and **(3)** gives dV/dt=0. Therefore, V, the volume of the CV, does not vary with time.

To simulate an accidental pollutant discharge (unsteady perturbations) we assume that the flow rate of the pollutant is negligible when compared to the flow rate of the river. Therefore, the flow rate of the accidental pollutant is not considered in the balance of volume; the flow rate out is equal to the flow rate in.

This simplification limits use of the simulation only when unsteady accidental discharges do not lead to drastic increases in the river flow rate. Therefore, before any simulation can begin, the ratios between the flow rates of these perturbation discharges and the river's flow rate have to be critically examined.

According to Chapra *et al.* (2003), there are three ways to determine a river's mean flow velocity - namely weirs, rating curves, and using Manning's formula. For this work, we chose to use the most common alternative given by **Eq. (4)**, Manning's formula. However, it is very easy to substitute this with another formulation as follows:

$$U = \frac{1}{n} R_h^{2/3} I_o^{1/2} \quad (4)$$

where U: cross-sectional average velocity (L/T); n: roughness coefficient ($T/L^{1/3}$); R_h: hydraulic radius (L); and I_o: longitudinal bottom slope (L/L).

For a simpler representation of the mass balance, we assume one-dimensional water flow, for which the concentration of any variable remains constant across each flow section. The resulting partial differential equation derived from the mass balance is as follows:

$$\frac{\partial C}{\partial t} = -\frac{1}{A_t}\frac{\partial (QC)}{\partial x} + \frac{1}{A_t}\frac{\partial}{\partial x}\left(D_L A_t \frac{\partial C}{\partial x}\right) \pm \frac{S}{V} \pm \frac{W}{V} \quad (5)$$

where S: sources or sinks (M/T); C: concentration of a variable (M/L^3); A_t: area of the flow section (L^2); D_L: longitudinal dispersion coefficient (L^2/T); and W: sources of pollution or sinks of pumping water (M/T).

The term S, sources or sinks, represents the contribution of the physical, chemical, and/or biological processes responsible for the production and/or consumption of the mass of the variables under simulation. All of the processes modeled are shown in **Table 1**.

To simulate water temperature, a thermal energy balance is calculated for control volume. This energy balance is very similar to the mass balance stated above.

For the thermal (internal) energy balance, both in and out flows of energy are considered. They are associated with the temperatures of the pollutant discharges, linked to the outflow of energy connected to water pumping, and linked to sources and sinks of other forms of energy exchange between the water and the environment.

The third part is modeled upon the combination of five processes: 1. Short wave solar radiation; 2. Long wave atmospheric radiation; 3. Short wave radiation emitted by the water; 4. Air-water convection; and 5. Evaporation-condensation. Processes 1 and 2 are modeled as sources of thermal energy; process 3 is modeled as a sink of thermal energy; processes 4 and 5 represent either sources or sinks, depending upon the sign of the temperature difference (water minus air

temperature). These mathematical formulations are also presented in Appendix A.

The resulting partial differential equation derived from the balance of thermal energy is as follows:

$$\frac{\partial T}{\partial t} = -\frac{1}{A_t}\frac{\partial (QT)}{\partial x} + \frac{1}{A_t}\frac{\partial}{\partial x}\left(D_L A_t \frac{\partial T}{\partial x}\right) \pm \frac{S_c}{V} \pm \frac{W_c}{V} \quad (6)$$

where S_c: sources or sinks of thermal energy (ML^2/T^3); T: water temperature (Θ); and W_c: polluting sources or water extraction (ML^2/T^3).

METHODS FOR SOLVING MASS AND THERMAL ENERGY TRANSPORT EQUATIONS

In its explicit form, the method of finite differences is used for spatial discretization of the equations. Time-partial differentiations are discretized using the fourth order Runge-Kutta method or Euler's method.

Figure 2 illustrates these operations. The letter "i" is used to denote position, and the letter "k" is used for the time variable. Terms such as C_i^k and T_i^k correspond to concentration and temperature at position "i" at time "k". Arrows with origins at time "k" indicate that the variables at time "k+1" have been calculated using the values found for the preceding moment.

In the explicit scheme, the space-wise discretization of first order differentials (advective term) and second order differentials (diffusive terms) was accomplished by backward and central finite differences, respectively. In **Eqs (7)** and **(8)**, "f" is a function that represents either C(x,t), or T(x,t). This approximation carries a local truncation error on the order of Δx.

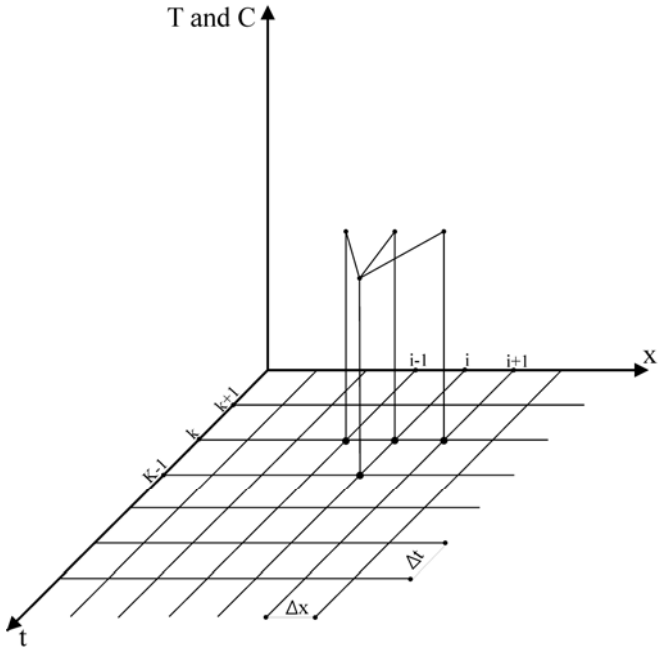

Fig. 2 Computational grid.

As previously stated, the software used for this modeling (Vensim PLE®) offers the user the choice of using either the fourth order Runge-Kutta method or the Euler method to calculate how the variables depend upon time. The software does all the work involved in the discretizations discussed in the previous paragraphs.

$$\frac{\partial f}{\partial x} = \frac{f_i^k - f_{i-1}^k}{\Delta x} \quad (7)$$

$$\frac{\partial^2 f}{\partial x^2} = \frac{f_{i+1}^k - 2f_i^k + f_{i-1}^k}{\Delta x^2} \quad (8)$$

By substituting **Eqs (7)** and **(8)** into **(5)** and **(6)**, the basic forms for the nodes were obtained **Eqs (9)** and **(10)**. The parameters A_t, D_L, S, S_c, W, and W_c were evaluated for existing conditions at the node (i, k).

$$\frac{dC}{dt} = -\frac{1}{A_{t_i}^k}\frac{Q_i^k C_i^k - Q_{i-1}^k C_{i-1}^k}{\Delta x} + \frac{1}{A_{t_i}^k}\frac{D_{L_i}^k A_{t_i}^k}{\Delta x} \frac{(C_{i+1}^k - 2C_i^k + C_{i-1}^k)}{\Delta x} \pm \frac{S_i^k}{\Delta x A_{t_i}^k} \pm \frac{W_i^k}{\Delta x A_{t_i}^k} \quad (9)$$

$$\frac{dT}{dt} = -\frac{1}{A_{t_i}^k}\frac{Q_i^k T_i^k - Q_{i-1}^k T_{i-1}^k}{\Delta x} + \frac{1}{A_{t_i}^k}\frac{D_{L_i}^k A_{t_i}^k}{\Delta x} \frac{(T_{i+1}^k - 2T_i^k + T_{i-1}^k)}{\Delta x} \pm \frac{S_{c_i}^k}{\Delta x A_{t_i}^k} \pm \frac{W_{c_i}^k}{\Delta x A_{t_i}^k} \quad (10)$$

The numerical solution for the one-dimensional transport differential equation using the method of finite differences necessarily carries numerical errors. They manifest themselves in several different ways, including rounding errors, instability, lack of symmetry, and numerical dispersion. Numerical dispersion is the most important, as shown by Wang & Lacroix (1997).

Using an analysis based on a Taylor series expansion, truncated after its second term, numerical dispersion can be estimated as follows:

$$D_n = \frac{\Delta x}{2} U - \frac{U^2 \Delta t}{2} \quad (11)$$

MASS BALANCE FOR SEDIMENT

The mathematical expressions used to model the flux of nutrients to and from the sediment and to model the benthonic demand of oxygen are based on studies by Di Toro (2001) and Chapra *et al.* (2007) that developed the QUAL2K EPA model.

Table 1. Sources and sinks for the water quality variables

Variables	Sources [M/T]	Sinks [M/T]
DO	Reaeration and photosynthesis	Respiration; degrading of carbonaceous organic matter; nitrification; and sediment oxygen demand.
Carbonaceous biochemical oxygen demand	Dissolution of detritus	Sedimentation; denitrification; and degradation of carbonaceous organic matter
Organic nitrogen (No)	Dissolution of detritus	Ammonification
Ammonia (Na)	Bottom algae and phytoplankton respiration	First stage nitrification; photosynthesis by bottom algae and phytoplankton
Nitrite (Ni)	First stage nitrification	Second stage nitrification
Nitrate (Nn)	Second stage nitrification	Denitrification; photosynthesis by bottom algae and phytoplankton
Organic phosphorus (Fo)	Dissolution of detritus	Hydrolysis
Inorganic phosphorus (Fi)	Bottom algae and phytoplankton respiration	Bottom algae and phytoplankton respiration
Alkalinity (Al)	Photosynthesis (nitrate used as substrate); respiration (ammonia used as substrate); and denitrification	Photosynthesis (ammonia used as substrate); respiration (nitrate used as substrate); and nitrification
Total coliforms (TC)	-	Death due to physical factors; and sedimentation
Zooplankton (Z)	Growth from grazing	Respiration
Phytoplankton (F)	Growth due to environmental factors: sunlight, temperature and nutrients	Respiration and grazing
Inorganic solid (Si)	-	Sedimentation
Bottom algae (A)	Growth due to environmental factors: sunlight, temperature and nutrients	Respiration and death
Detritus (D)	Death of bottom algae and phytoplankton grazing	Dissolution and sedimentation
Total inorganic carbon (TIC)	Phytoplankton and bottom algae respiration; organic carbon oxidation; and reaeration	Photosynthesis by phytoplankton and bottom algae
pH	Ratio of alkalinity to total inorganic carbon	Ratio of alkalinity to total inorganic carbon

The mathematical formulations used to quantify all of these sources and sinks are presented in Appendix A.

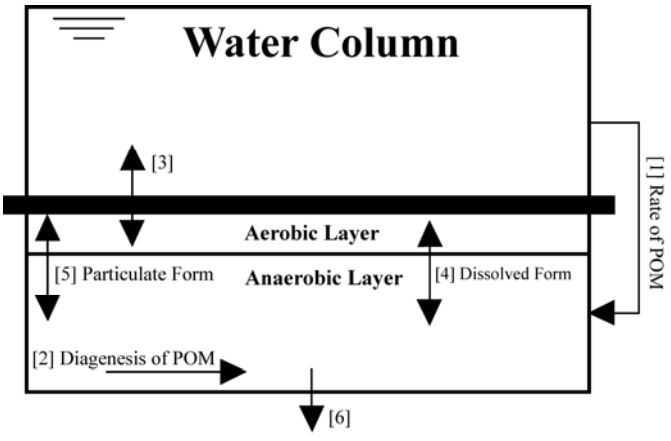

Fig. 3 Schematic of the two layers of sediment and the processes occurring in the sediment. Source: Data from Di Toro (2001).

The sediment was divided into two layers; the first was aerobic (H_a) with a thickness of 1 mm, and the second was anaerobic (H_{an}) with a thickness of 10 cm (**Fig. 3**).

As shown in **Fig. 3**, six processes may be responsible for changes in concentrations occurring in the sediment. Five of them involve mass transport; the sixth involves a biochemical reaction. These processes are as follows: (1) Deposition of particulate organic matter (POM) in the aerobic layer, from the sedimentation of detritus (D) and the carbonaceous BOD; (2) Diagenesis, which is the conversion of organic matter into more soluble forms, such as, CH_4, NH_4^+ and PO_4^{-3} (used to account for inorganic phosphorus); (3) Diffusion at the interface of the aerobic layer and the water column; (4) Diffusion of soluble substances across the interface of the two layers; (5) Pseudo-diffusive transport of particulate substances across the two layers; and (6) Sinking of soluble or particulate substances by incorporation into the soil.

Processes (4) and (5) were positively influenced by the presence of benthonic organisms. Thus, the coefficients of molecular diffusion, as used when there is no micro-fauna in the sediment, may be augmented two- or three-fold due to the presence of benthonic organisms.

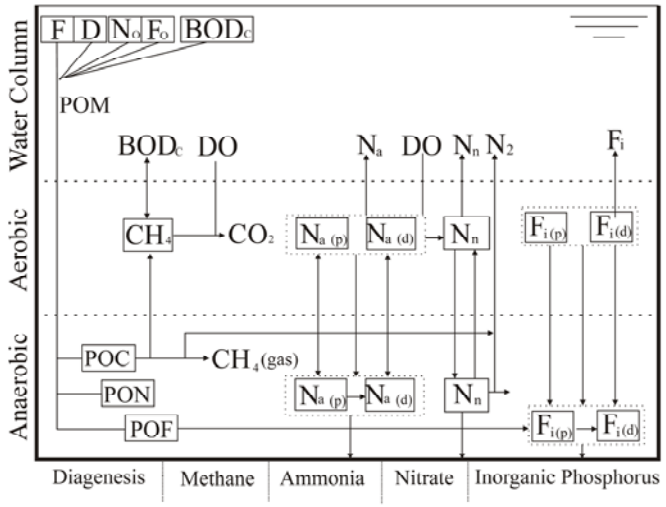

Fi. 4 Flux of nutrients in the sediment.

Figure 4 shows a detailed diagram of the nutrient fluxes and dissolved oxygen consumption in the sediment. The letters "p" and "d" are used to represent parcels in the particulate and dissolved forms, respectively. **Figure 4** shows that the particulate organic carbon (POC) freed in the anaerobic layer may originate from the sedimentation of particulate detritus and from the particulate carbonaceous BOD. On the other hand, the particulate organic nitrogen (PON) and the particulate organic phosphorus (POP) are derived exclusively from the sedimentation of particulate detritus.

In the anaerobic layer, organic carbon, nitrogen, and phosphorus are transformed by mineralization reactions into methane, ammonia nitrogen and inorganic phosphorus, respectively. These constituents are transported to the aerobic layer, where methane and ammonia nitrogen can be oxidized, thereby determining the demand for dissolved oxygen.

EXAMPLES OF APPLICATIONS

Application example 1

The first example shows the importance of correcting for numerical dispersion when simulating water quality during an accidental spill. The viability of the numerical solution is established by comparing it to the exact analytical solution of the advection-dispersion **Eq. (12)**.

$$C(x,t) = \frac{M}{A_t 2\sqrt{\pi D_L t}} \exp - \left\{ \frac{[(x - x_1) - Ut]^2}{4 D_L t} \right\} \quad (12)$$

where M: mass of the substance (pollutant) (M); x: position of interest (L); x_1: position of the substance spill (L); and t: time (T).

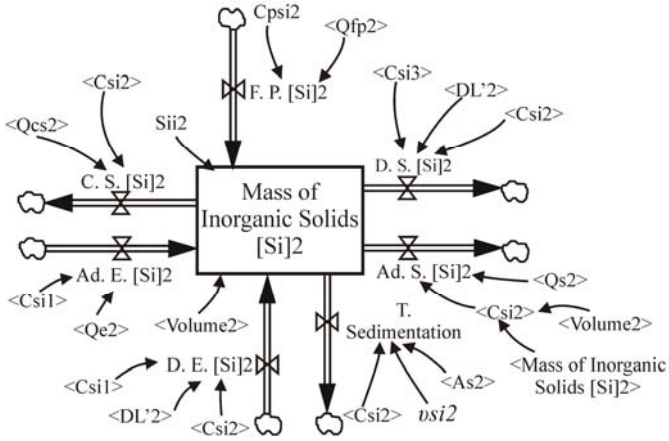

Fig. 5 Mass balance for the inorganic solids parameter.

Terms associated with sources and sinks are not included in this equation; therefore, it can be used only to simulate the transport of conservative substances. For this example, we considered the substance to be an inorganic solid not subjected to sedimentation, which would act as a sink.

Figure 5 is used, with a mass balance for inorganic solids in a control volume, to better understand how **Eqs (9)** and **(10)** were implemented into the Vensim PLE® program. Variable number two indicates that control volume number two is under study, following control volume number one and preceding control volume number three. Arrows with a single line connect variables, indicating interdependence. For example, to determine the concentration of Csi 2, volume two and the mass of Si two are needed, as indicated by the arrows in the lower right corner of **Fig. 5**. Arrows with double lines indicate flow rates in and out of a control volume. For instance, the two horizontal arrows at the bottom account for advective contribution of Si to and from volume two: (Ad. E.) and (Ad. S.).

The hypothetical river used for this simulation is 2 km long and received an instantaneous load of 5 kg of inorganic solids dumped at a position of x = 500 m. We assumed a flow rate of 3.456×10^6 m^3/d, a width of 60 m, and a depth of 1.0 m. Also, we assumed that the coefficient of longitudinal dispersion D_L is equal to 3.6×10^6 m^2/d, the Manning coefficient is 0.0456, and the channel slope is 0.001. These parameters were constant for the stretch of river under simulation, and had to be input by the user; thereafter, the model determined the values of other parameters, such as the area of the water section (60 m^2 for a rectangular shape) and the mean flow velocity (57,456 m/d or 0.665 m/s).

This 2 km river stretch was divided into 20 control volumes (VC) with lengths of Δx = 100 m. The time increment Δt was established as $\Delta t = 10^{-5}$ d. To eliminate the effects of numerical dispersion, which is predicted by **Eq. (11)** to be $D_n = 2.86\times10^6$ m^2/d, this value was subtracted from the original coefficient of

longitudinal dispersion, resulting in $D_L = 0.74\times10^6$ m^2/d, or $D_L = 7.4\times10^7$ m^2/d.

The background concentration of the water body was assumed to be zero; dumping the inorganic solid at time t = 0 raised the concentration of CV 5 to 0.833 mg/L.

Figure 6 shows the longitudinal concentration profiles along the 2 km for two moments, t = 0.007 d and t = 0.02 d. The two solid lines correspond to the analytical solutions; the marks correspond to the numerical results of the model's simulation.

The results produced by the two solutions are very similar. For most of the length of the river, the absolute difference is less than 0.005 mg/L. Only for the stretch of 700 m to 1,100 m at time t = 0.007 d did differences reach values of 0.010 mg/L.

A second simulation of the same case was run without correcting for numerical dispersion. **Figure7** shows the results for the same instants. The additional effects of numerical dispersion are readily apparent.

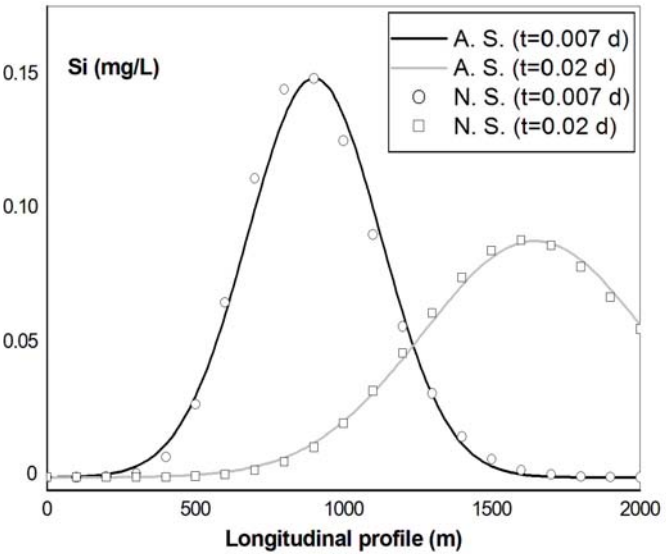

Fig. 6 Longitudinal profiles for an inorganic solid. Analytical solution and model prediction corrected for numerical dispersion.

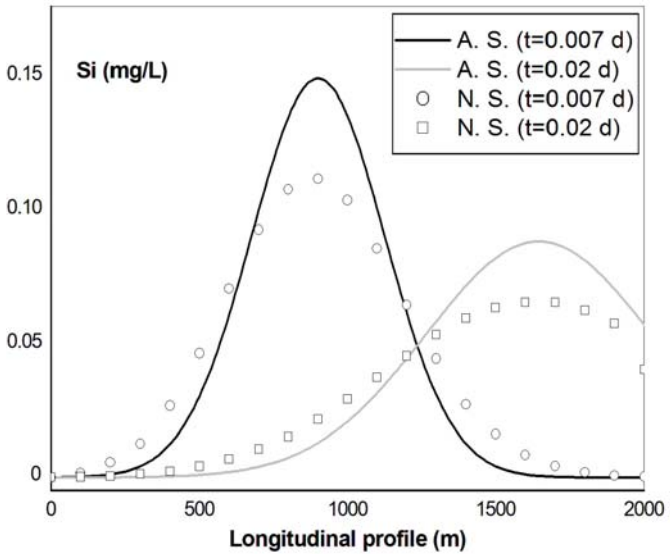

Fig.7 Longitudinal profiles for an inorganic solid. Analytical solution and model prediction not corrected for numerical dispersion.

Application example 2

The objective of the second example is to demonstrate the ability of the new model to simulate a water quality profile under steady conditions. Its results for a DO profile are compared with the results of simulation performed with model QUAL2K. Data for this study were produced by Gonçalves *et al.* (2012) in his report on the qualitative and quantitative monitoring of rivers of the São Simão basin in the state of São Paulo, Brazil.

Gonçalves *et al.* (2012) studied a fluvial segment of 11,41 km in length, running from its origin to sampling station S6 (**Fig. 8**). This segment was divided into eight stretches, taking into consideration the flow characteristics, the kinetics of the process, and the availability of quantitative and qualitative pieces of information. Each stretch was subdivided into control volumes (computational elements) with lengths of 0.5 km each.

Both QUAL2K and Vensim PLE were calibrated and verified in steady-state mode using average conditions during March 2005 to March 2006. The values of system coefficients were based on the typical values cited in the model documentation (Brown & Barnwell, 1987; Chapra *et al.* 2007). All values of system coefficients used in QUAL2K were same as those in Vensim PLE. This strategy permitted us to adequately identify the reasons for inconsistencies in the two DO profiles predicted by the different models. Table 2 shows the resulting values for several coefficiens, namely coefficient of deoxygenation K_d, coefficient of surface reaeration K_2, and settling rate K_s.

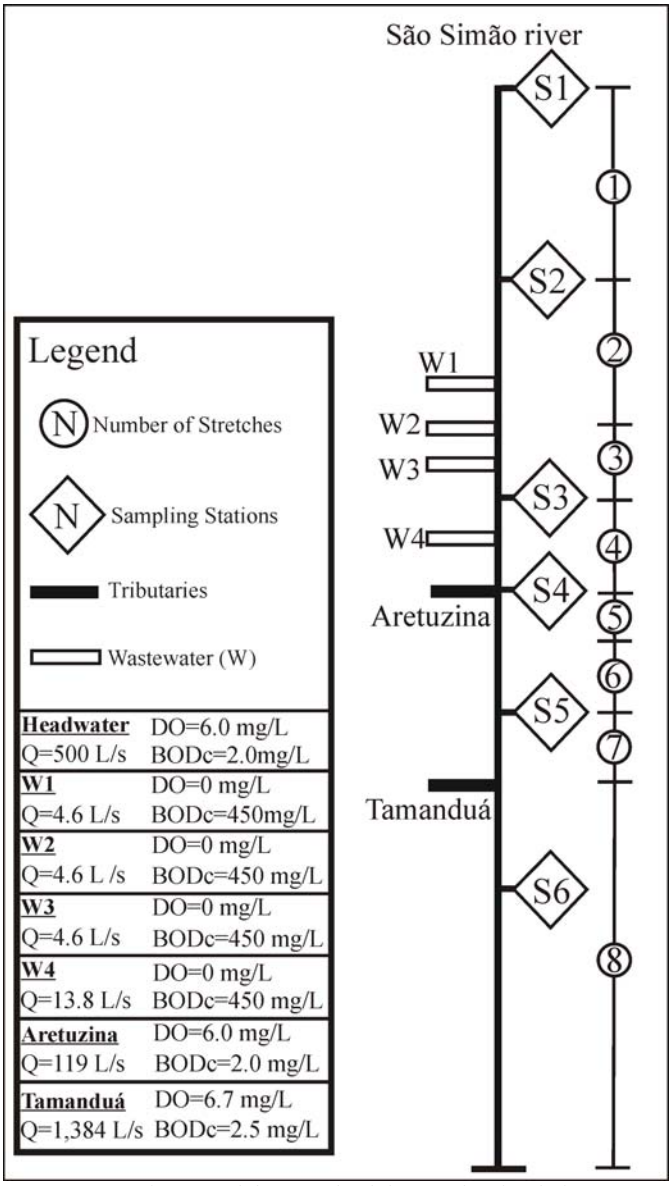

Fig. 8 Diagram of the stretch of river under simulation.

Both QUAL2K and Vensim PLE model results were compared with fields measurements in figure (**Fig. 9**). Field measurements are displayed as mean and 95% confidence intervals. **Figure 9** shows that both models represent the field data quite well, since the profiles are quite similar.

Table 2. Parameters for DO modeling

Stretch	K_d (d^{-1})	K_2 (d^{-1})	K_s (d^{-1})
1	0.3	0.8	0.1
2	0.3	0.8	0.1
3	1.0	0.3	0.3
4	1.0	0.3	0.3
5	1.0	0.3	0.3
6	1.0	0.3	0.3
7	1.0	1	0.1
8	1.0	1	0.1

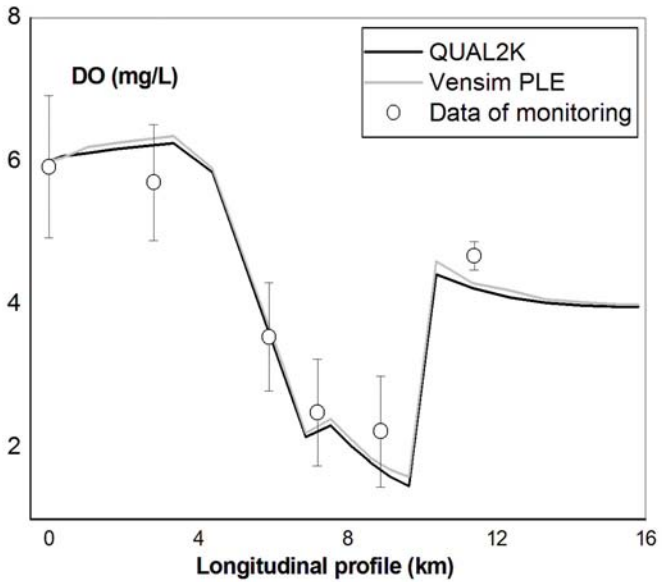

Fig. 9 DO concentration profiles resulting from simulations with QUAL2K and Vensim PLE®.

Application example 3

In this example, we ran a simulation to showcase some of the tools available in Vensim PLE®. For instance, it is possible for the software to represent any time variation for a pollutant discharge. A simulation was run for the two classical water quality parameters DO and carbonaceous BOD. The concentrations of the other parameters present in the model were assumed to be zero.

The hypothetical river modeled in this example is 20 km long, has a flow rate of 69 120 m^3/d, a width of 1.5 m, and a depth of 0.8 m. The coefficient of longitudinal dispersion was 1.0368×10^7 m^2/d, the bottom slope was 0.001, the Manning coefficient was 0.0465, and the flow average velocity was 0.36 m/s. As seen in application 1, the model automatically corrects for any numerical dispersion.

A factory discharges an effluent at x = 500 m in a cyclic manner (every 2.4 h, or every 0.1 d for 15 min), with a flow rate of 8,640 m^3/d, carbonaceous BOD concentration of 2 000 mg/L, and DO concentration of 0.5 mg/L. The effluent flow rate was introduced into the program using a *pulse train*, which is a feature of Vensim PLE® (**Fig. 10**). In the figure, "Q_{fp}" represents the flow rate of the source of the pollutant.

Fig. 10 shows that the length of the simulation was one day. The first pulse of pollution occurred at 0.1 d and the last time 0.9 d, and there were a total of nine pulses.

The initial conditions for the water body were 0 mg/L of carbonaceous BOD and 7 mg/L of DO, adopted for the two parameters in all of the CVs and as boundary conditions upstream and downstream of the set of CVs.

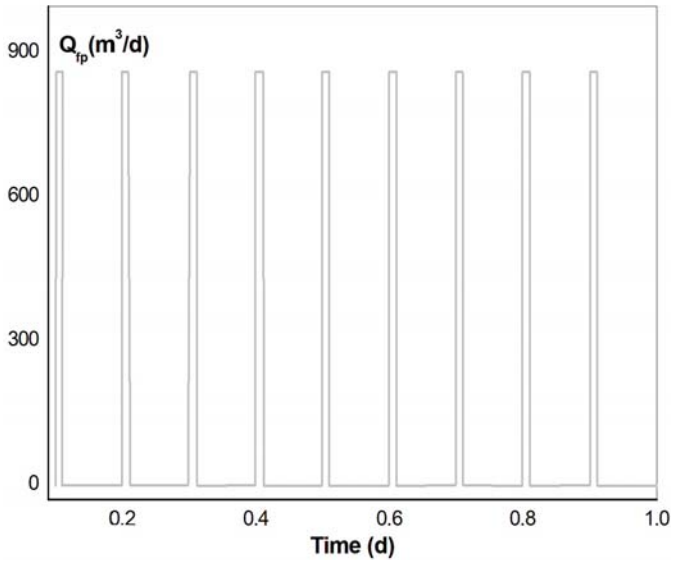

Fig. 10 Flow rate variation as a function of time.

Figure 11 shows the results of a simulation of the carbonaceous biochemical demand concentration for different positions along the river. From position 500 m to position 9,000 m, the peak BODc concentration dropped ΔC_{BODc} = 153 – 24.3 = 128.7 g/m^3. This attenuation along the longitudinal river profile was the result of the combined effects of longitudinal dispersion, biological degradation of organic matter, and sedimentation; the last two processes were sinks for BODc.

The DO concentration is presented in the same manner in **Fig. 12**. At position x = 500 m, the DO concentration reached a saturation level (7.5 mg/L) at the midpoint of times between effluent discharges. The same did not occur in the downstream positions, as the utilization of oxygen surpassed its reposition by surface reoxygenation.

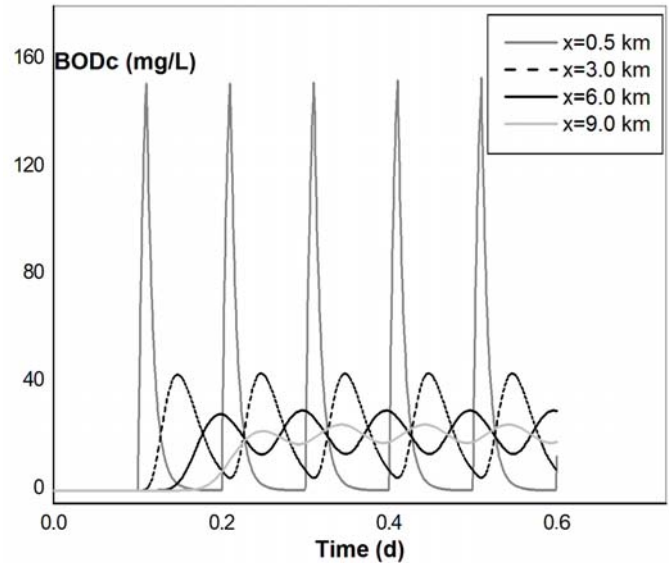

Fig. 11 Graphical outputs for C_{BODc}(x) as functions of time.

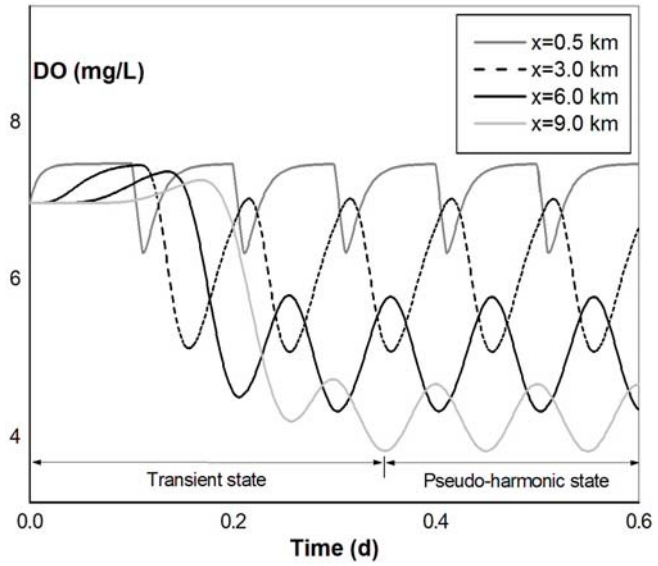

Fig. 12 Graphical outputs for C_{DO}(x) as functions of time.

Another interesting point from **Fig. 12** is the transition from a transient state to a pseudo-harmonic state, with constant minimum and maximum values for the oscillating DO parameter. Notice that the same type of transition occurs for BODc in **Fig. 11**.

Application example 4

In this example, the behaviors of six water quality parameters were analyzed, namely organic nitrogen (N_o), ammonia nitrogen (N_a), nitrite (N_i), nitrate (N_n), organic phosphorus (F_o), and inorganic phosphorus (F_i).

The river simulated in this example has a length of 160 km, flow rate of 25 920 m^3/d, width of 2.2 m, depth of 0.4 m, water temperature of 32^o C, bottom slope of 0.0052, a Manning's roughness of 0.05, and flow velocity of 0.66 m/s.

For t = 0 (initial condition) and at x = 0 and x= 160 km (boundary conditions), the concentrations of all forms of nitrogen and phosphorus compounds were zero.

There was a continuous discharge of polluted water at position x = 1 000 m. Its flow rate was 2 000 m^3/d with an organic nitrogen concentration of 15 mg/L and a 5 mg/L concentration of organic phosphorus.

For simplicity, the concentration of other water quality parameters, such as phytoplankton and algae, which can contribute to the production and/or use of nitrogen and phosphorus compounds, were assumed to be zero. Therefore, the only source of organic nitrogen and phosphorus was the polluting discharge. The results of the simulation are shown in **Fig. 13**.

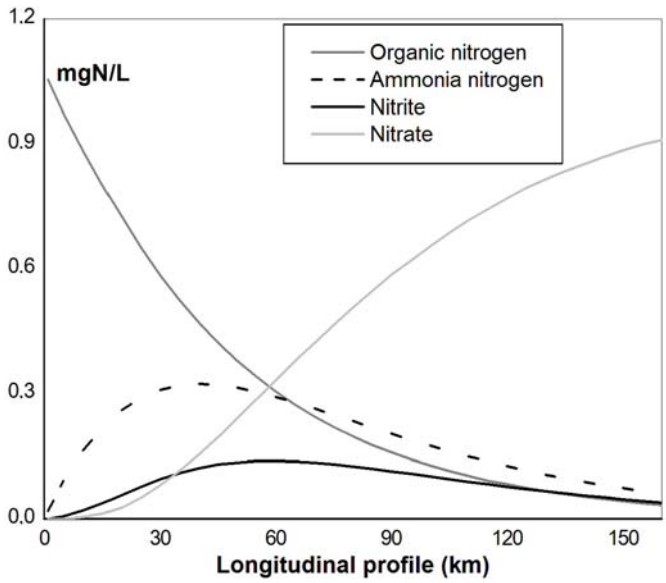

Fig. 13 Concentration profiles for the forms of nitrogen compounds along the simulated river course

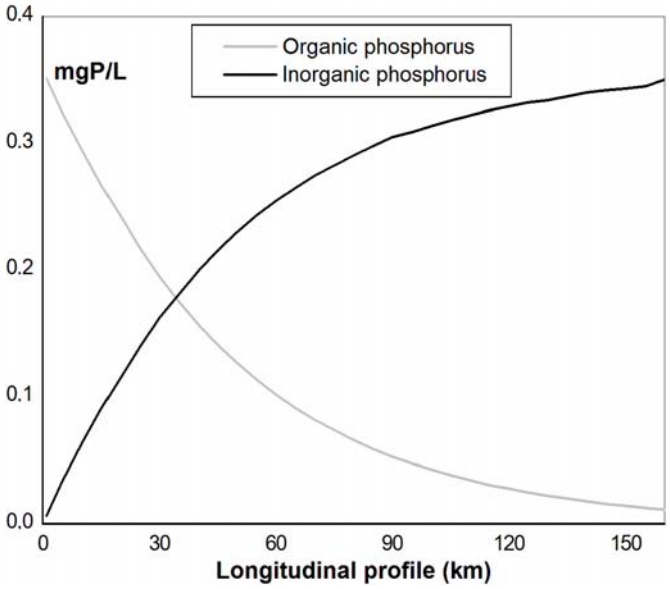

Fig. 14 Concentration profiles for the forms of phosphorus compounds along the simulated river course

Figure 13 shows that the concentration of organic nitrogen decreases along the course of the river as it is transformed into ammonia. In this process (ammonification), the organic nitrogen is consumed as ammonia nitrogen is produced; however, ammonia nitrogen in the presence of dissolved oxygen is transformed into nitrite (first stage nitrification), and nitrite is then transformed into nitrate (second stage nitrification). In this example, the DO concentration was kept at a level of 7.5 mg/L.

The last reaction occurs very quickly; therefore, the nitrite concentration in the water body fails to reach elevated values. The kinetic coefficient for the conversion of nitrite into nitrate is larger than the kinetic coefficient for the conversion of ammonia into nitrite. Nitrate may be transformed into gaseous nitrogen if the environment was anoxic, which was not the case in this example.

One can verify that the concentrations of N_a, N_i, and N_n, at position x = 160 km add up to the difference between N_o at x = 1 km and x = 160 km. The organic nitrogen is sequentially transformed into ammonia, then into nitrite, and finally into nitrate nitrogen.

Figure 14 illustrates the concentration profiles of organic and inorganic phosphorus. It shows that, unlike what happened to the nitrogen compounds, the curves for the decay of organic phosphorus and production of inorganic phosphorus are symmetrical mirror images of one another. All organic phosphorus consumed along the river is transformed into inorganic phosphorus; in other words, the sink of F_o corresponds to an equal source of F_i.

CONCLUSION

The model discussed in this paper corrects for limitations in similar products that have been discussed elsewhere in the literature, such as the QUAL family. The reasons for this model are as follows: (1) the user can easily change the internal structure of the model, introducing equations that better represent reality; (2) the model can be operated very easily under non-steady conditions, as the Vensim PLE® software package includes tools, such as *pulse train* and *lookup*, that facilitate the representation of pollutant discharges for any time variation profile; and (3) the user can choose to use different values for the many coefficients involved in the processes at any position in the body of water.

Numerical errors were corrected satisfactorily, yielding good results when a relatively small spatial discretization was used. It is important to note that the model can internally correct for any computational numerical errors.

The simulated results for the DO and BODc of unsteady regimes were as expected; however, local field work, including the monitoring and evaluation of water quality in the presence of instantaneous pollutant discharges, is recommended to calibrate the model and thereby ensure a faithful response to transient disturbances.

Steady state simulations for nitrogen and phosphorus compounds also ran as expected. Organic nitrogen was transformed into nitrate almost completely along the modeled course.

The results suggest that using Vensim PLE® as a basic tool to develop environmental models is an excellent option.

Acknowledgement

This study was supported by the Brazilian National Council for Scientific and Technological Development - CNPq.

APPENDIX A. EQUATIONS

The following are equations that describe the "sources and sinks" for each water quality variable.

Temperature (T)

$$\frac{VC_e\rho dT}{dt} = S_c = J\,A_s \quad (13)$$

$$J = J_{oc} + J_{ol} - (J_{a,ol} + J_c + J_{ev/co}) \quad (14)$$

$$J_{oc} = J_{topo}\quad 0.24 + 0.58\frac{n}{N_m} \quad (15)$$

$$J_{a,ol} = \varepsilon\sigma(T+273)^4 \quad (16)$$

$$J_c = c_1(19 + 0.9U_v^2)(T - T_{ar}) \quad (17)$$

$$J_{ev/co} = (19 + 0.95U_v^2)(e_s - e_{ar}) \quad (18)$$

$$J_{ol} = \sigma(T_{ar}+273)^4\,(A + 0.031\sqrt{e_{ar}})(1 - C_r) \quad (19)$$

Total Coliforms (TC)

$$\frac{dN_{CT}}{dt} = S_{CT} = -TS_{CT} - TM_{CT} \quad (20)$$

$$TS_{CT} = K_{Sct}VC_{ct} \quad (21)$$

$$TM_{CT} = (K_r + K_b)N_{CT} \quad (22)$$

$$K_b = 0.8\theta_{CT}^{(T-20)} \quad (23)$$

$$K_r = \frac{(\alpha J_{ocm})}{K_e H}\left(1 - e^{-K_e H}\right) \quad (24)$$

$$K_e = 0.052C_{si} + 0.174C_d + 0.000031C_f \quad (25)$$

Phytoplankton (F)

$$\frac{dM_F}{dt} = S_F = TC_F - TR_F - TG_F \quad (26)$$

$$TR_F = \mu_{rf}\theta R_f^{(T-20)}M_F F_f \quad (27)$$

$$F_f = 1 - e^{-K_{resf}C_{od}} \quad (28)$$

$$TG_F = [\frac{C_f}{(K_{s_g} + C_f)}C_g\theta G_z^{(T-20)}C_z]\,M_F \quad (29)$$

$$TC_F = K_{cf}(T,N,L)M_F \quad (30)$$

$$K_{cf} = K_{cf}(T)\times K_{cf}(N)\times K_{cf}(L) \quad (31)$$

$$K_{cf}(T) = C_{rf\,máx}\theta F^{(T-20)} \quad (32)$$

$$K_{cf}(L) = \frac{2.718f}{K_e H}(e^{-\alpha_1} - e^{-\alpha_0}) \quad (33)$$

$$\alpha_1 = \frac{J_{oc_m}}{J_{oc_o}}e^{(-K_e H)} \quad (34)$$

$$\alpha_0 = \frac{J_{oc_m}}{J_{oc_o}} \quad (35)$$

$$K_{cf}(N) = \frac{N}{N + K_s} \quad (36)$$

$$K_{cf}(N) = \min\left\{\frac{(C_{na} + C_{nn})}{(C_{na} + C_{nn} + K_{s_{nf}})}; \frac{C_{fi}}{(C_{fi} + K_{s_{fi}})}\right\} \quad (37)$$

Zooplankton (Z)

$$\frac{dM_Z}{dt} = S_Z = TC_Z - TR_Z \quad (38)$$

$$TC_Z = TG_F R_{ca} E_{fg} \quad (39)$$

$$TR_Z = K_{rz}\theta R_Z^{(T-20)}M_Z \quad (40)$$

Bottom Algae (A)

$$\frac{dM_A}{dt} = S_A = TC_A - TR_A - TM_A \quad (41)$$

$$TC_A = K_{ca}A_s \quad (42)$$

$$TM_A = \mu_{ra}F_a M_A \quad (43)$$

$$F_a = F_f \quad (44)$$

$$TR_A = K_{ma}M_A \quad (45)$$

Detritus (D)

$$\frac{dM_D}{dt} = S_D = TP_D - TD_{iD} - TS_D \quad (46)$$

$$TS_D = C_d A_s \upsilon_d \quad (47)$$

$$TD_{i_D} = K_{di}\theta D_i^{(T-20)}M_D \quad (48)$$

$$TP_D = TM_A + [(1 - E_{fg})R_{da}TG_F] \quad (49)$$

Inorganic Solids (S_i)

$$\frac{dM_{Si}}{dt} = S_{Si} = -TS_{Si} \quad (50)$$

$$TS_{Si} = C_{si}A_s\upsilon_{si} \quad (51)$$

Organic Nitrogen (N_o), Ammonium Nitrogen (N_a), Nitrite (N_i), and Nitrate (N_n)

$$\frac{dM_{No}}{dt} = S_{No} = TP_{No} - TD_{No} \quad (52)$$

$$TP_{No} = TD_{iD}R_{nd} \quad (53)$$

$$TD_{No} = K_{oa}\theta A_m^{(T-20)}M_{No} \quad (54)$$

$$\frac{dM_{Na}}{dt} = S_{Na} = TP_{Na} - TA_{Na} - TN_{Na} \quad (55)$$

$$TP_{Na} = TD_{No} + (R_{nd}TR_A) + (R_{na}TR_F) \quad (56)$$

$$TA_{Na} = F_{am}(R_{na}TC_F + R_{nd}TC_A) \quad (57)$$

$$F_{am} = \frac{C_{na}C_{nn}}{(Kp_{na} + C_{na})(Kp_{na} + C_{nn})} + \frac{C_{na}Kp_{na}}{(Kp_{na} + C_{nn})(C_{na} + C_{nn})} \quad (58)$$

$$TN_{Na} = K_{ai}\theta N^{(T-20)}M_{Na}F_{Nai} \quad (59)$$

$$F_{Nai} = 1 - e^{-K_{ini}C_{od}} \quad (60)$$

$$\frac{dM_{Ni}}{dt} = S_{Ni} = TN_{Na} - TN_{Ni} \quad (61)$$

$$TN_{Ni} = K_{in}\theta N^{(T-20)}M_{Ni}F_{Nii} \quad (62)$$

$$F_{Nii} = 1 - e^{-K_{inn}C_{od}} \quad (63)$$

$$\frac{dM_{Nn}}{dt} = S_{Nn} = TN_{Ni} - TA_{Nn} - TD_{esNn} \quad (64)$$

$$TD_{esNn} = K_{des}\theta N^{(T-20)}M_{Nn}(1 - F_{des}) \quad (65)$$

$$F_{des} = 1 - (1 - e^{-K_{ides}C_{od}}) \quad (66)$$

$$TA_{Nn} = (1 - F_{am})(R_{na}TC_F + R_{nd}TC_A) \quad (67)$$

Organic (F_o) and Inorganic (F_i) Phosphorous

$$\frac{dM_{Fo}}{dt} = S_{Fo} = TP_{Fo} - TD_{Fo} \quad (68)$$

$$TP_{Fo} = TD_{iD}R_{pd} \quad (69)$$

$$TD_{Fo} = K_{oi}\theta H_{fo}^{(T-20)}M_{Fo} \quad (70)$$

$$\frac{dM_{Fi}}{dt} = S_{Fi} = TP_{Fi} - TA_{Fi} \quad (71)$$

$$TP_{Fi} = TD_{Fo} + (R_{pd}TR_A) + (R_{pa}TR_F) \quad (72)$$

$$TA_{Fi} = (R_{pa}TC_F + R_{pd}TC_A) \quad (73)$$

Carbonaceous Biochemical Demand (BOD_c)

$$\frac{dM_{DBOc}}{dt} = S_{DBOc} = TP_{DBOc} - TD_{DeDBOc} - TD_{DesDBOc} - TS_{DBOc} \quad (74)$$

$$TP_{DBOc} = TD_{iD}R_{cd}R_{oc} \quad (75)$$

$$TD_{eDBOc} = K_d\theta D^{(T-20)}M_{DBOc}F_{DBOci} \quad (76)$$

$$F_{DBO_ci} = 1 - e^{-K_{idegr}C_{od}} \quad (77)$$

$$K_d = K_1 + i\ \frac{U}{H} \quad (78)$$

$$TD_{esDBOc} = TD_{esNn}R_{ondes} \quad (79)$$

$$TS_{DBOc} = Ks_{DBOc}\theta S_{DBOc}^{(T-20)}M_{DBOc} \quad (80)$$

Dissolved Oxygen (DO)

$$\frac{dM_{OD}}{dt} = S_{OD} = TF_{OD} + TR_{eOD} - TR_{OD} - TD_{esoOD} - TN_{OD} \quad (81)$$

$$TR_{eOD} = K_2\theta R_e^{(T-20)}(C_S - C_{od})V \quad (82)$$

$$TR_{OD} = \underbrace{(TR_FR_{ca}R_{oc})}_{\text{Phytoplankton}} + \underbrace{(TR_AR_{cd}R_{oc})}_{\text{Bottom Algae}} \quad (83)$$

$$TD_{esoOD} = TD_{eDBOc} = K_d\theta D^{(T-20)}M_{DBOc}F_{DBO_ci} \quad (84)$$

$$TN_{OD} = TN_{Na}R_{oni} + TN_{Ni}R_{onn} \quad (85)$$

$$TF_{OD} = \underbrace{(TC_FR_{ca}R_{oc})}_{\text{Phytoplankton}} + \underbrace{(TC_AR_{cd}R_{oc})}_{\text{Bottom Algae}} \quad (86)$$

Total Inorganic Carbon (TIC)

$$\frac{dM_{CIT}}{dt} = S_{CIT} = TR_{CIT} + TR_{eCO_2} + TD_{eCIT} - TF_{CIT} \quad (87)$$

$$TR_{eCO_2} = K_{CO_2}(C_{CO_2}s - C_{cit}F_o)V \quad (88)$$

$$TD_{eCIT} = TD_{eDBOc}R_{co}R_{mol,C} \quad (89)$$

$$TR_{CIT} = \underbrace{(TR_FR_{ca}R_{mol,C})}_{\text{Phytoplankton}} + \underbrace{(TR_AR_{cd}R_{mol,C})}_{\text{Bottom Algae}} \quad (90)$$

$$TF_{CIT} = \underbrace{(TR_FR_{ca}R_{mol,C})}_{\text{Phytoplankton}} + \underbrace{(TR_AR_{cd}R_{mol,C})}_{\text{Bottom Algae}} \quad (91)$$

Alkalinity (Al.)

$$\frac{dN_{Al.}}{dt} = S_{Al.} = TA_{Al.} + TD_{esAl.} - TD_{Al.} - TN_{iAl.} \quad (92)$$

$$TA_{Al.} = \underbrace{(F_{am}TR_FR_{ca}R_{mol,C}R[H^+],na)}_{\text{Phytoplankton}} + \underbrace{(F_{am}TR_AR_{cd}R_{mol,C}R[H^+],na)}_{\text{Bottom Algae}} + \underbrace{(1 - F_{am}TC_FR_{ca}R_{mol,C}R[H^+],nn)}_{\text{Phytoplankton}} + \underbrace{(1 - F_{am}TC_AR_{cd}R_{mol,C}R[H^+],nn)}_{\text{Bottom Algae}} \quad (93)$$

$$TD_{Al.} = \underbrace{(F_{am}TC_FR_{ca}R_{mol,C}R[H^+],na)}_{\text{Phytoplankton}} + \underbrace{(F_{am}TC_AR_{cd}R_{mol,C}R[H^+],na)}_{\text{Bottom Algae}} + \underbrace{(1 - F_{am}TR_FR_{ca}R_{mol,C}R[H^+],nn)}_{\text{Phytoplankton}} + \underbrace{(1 - F_{am}TR_AR_{cd}R_{mol,C}R[H^+],nn)}_{\text{Bottom Algae}} \quad (94)$$

$$TD_{esAl.} = TD_{esNn}R_{mol,N}R[H^+],des \quad (95)$$

$$TN_{i_{Al.}} = \left(TN_{Na} + TN_{Ni}\right) R_{mol,N} R[H^+], nitri \quad (96)$$

pH

$$pHa = 7.5 + 2\left(\frac{C_{al.}}{C_{cit}} - 1\right) + \frac{Ha_{Lim}}{1 + \frac{Ha_{Lim} - Ha_0}{Ha_0} e^{-K\left(\frac{C_{al.}}{C_{cit}} - A_0\right)}} + \frac{Ha_{Lim}}{1 + \frac{Ha_{Lim} - Ha_0}{Ha_0} e^{-K\left(\frac{C_{al.}}{C_{cit}} - A_1\right)}} + \frac{Ha_{Lim}}{1 + \frac{Ha_{Lim} - Ha_0}{Ha_0} e^{-K\left(\frac{C_{al.}}{C_{cit}} - A_2\right)}} \quad (97)$$

APPENDIX B. NOMENCLATURE

A: coefficient related to air temperature and to the actual solar radiation and clean sky solar radiation; range: 0.5 to 0.7 (non-dimensional) $A \approx 0.7$ for air temperatures of above 20° C.

A_0: coefficient for the beginning of the curve (non-dimensional).

A_1: coefficient for the middle of the curve (non-dimensional).

A_2: coefficient for the end of the curve (non-dimensional).

A_s: surface area for each control volume (cm^2).

c_1: Bowen's coefficient (mm Hg/°C).

$C_{al.}$: concentration of calcium carbonate ($mgCaCO_3/L$).

C_{ct}: concentration of total coliforms (N_{org}/L).

C_{cit}: concentration of total inorganic carbon (mol/L).

$C_{CO2}s$: saturation concentration of CO_2 in water (mol/L).

C_d: concentration of detritus (mgD/L).

C_e: specific heat (cal/g°C).

C_f: concentration of phytoplankton (mgA/L).

C_{fi}: concentration of inorganic phosphorus (mgP/L).

C_g: kinetic coefficient for zooplankton grazing (L/mgCd).

C_{na}: concentration of ammonium nitrogen (mgN/L).

C_{nn}: concentration of nitrate (mgN/L).

C_{od}: concentration of dissolved oxygen (mgO/L).

C_r: coefficient of reflection (non-dimensional).

$C_{rfmáx}$: coefficient for the maximum growth of phytoplankton (≈ 1.8); this value varies as a function of the phytoplankton species (1/d).

C_s: saturation concentration of dissolved oxygen (mgO/L).

C_{si}: concentration of inorganic solids (mg/L).

C_z: concentration of zooplankton (mgC/L).

e_{ar}: vapor pressure in the atmosphere (mm Hg).

E_{fg}: efficiency factor for grazing (non-dimensional).

ε: emissivity of water (≈ 0.97) (non-dimensional).

e_s: water vapor pressure (mm Hg).

f: photoperiod (non-dimensional).

F_a: factor of attenuation for bottom algae respiration (non-dimensional).

F_{am}: factor of preference for ammonium (non-dimensional).

F_{DBOci}: factor of correction (attenuation) of the coefficient of deoxygenation as a function of DO concentration (non-dimensional).

F_{des}: factor of correction (attenuation) of the coefficient of denitrification as a function of DO concentration (non-dimensional).

F_f: factor of correction (attenuation) of the coefficient of phytoplankton respiration as a function of DO concentration (non-dimensional).

F_{Nai}: factor of correction (attenuation) for the coefficient of first stage nitrification as a function of DO concentration (non-dimensional).

F_{Nii}: factor of correction (attenuation) for the coefficient of second stage nitrification as a function of DO concentration (non-dimensional).

F_o: fraction of free inorganic carbon [non-dimensional]

H: river depth (m).

Ha_0: initial value 1.05 (non-dimensional).

Ha_{Lim}: limiting value for growth; function of temperature (non-dimensional).

i: coefficient of activity in the bottom mud (non-dimensional).

$J_{a,ol}$: short wave radiation flux emitted by the water (cal/cm^2 d).

J_c: convective flux of thermal energy between the water and the atmosphere (cal/cm^2 d).

$J_{ev/co}$: flux of thermal energy eliminated from the water by evaporation, or gained by condensation (cal/cm^2 d).

J_{oc}: flux of short wave solar radiation (cal/cm^2 d).

J_{ocm}: average short wave solar radiation flux (cal/cm^2 d).

J_{oco}: optimal short wave solar radiation flux for phytoplankton growth (300 cal/cm^2 d).

J_{ol}: flux of long wave radiation from the atmosphere (cal/cm^2 d).

J_{topo}: flux of solar radiation at the upper layers of the atmosphere (cal/m^2 d), calculated as I_o senα; I_o is the solar constant, equal to 2.88×10^7 cal m^2/d; α is the inclination of solar rays to the horizontal.

K_{CO2}: coefficient of global transfer of CO_2 (1/d).

K: growth coefficient (≈27) (non-dimensional).

K_1: kinetic coefficient for deoxygenation (1/d).

K_2: coefficient of surface reoxygenation (1/d).

K_{ai}: kinetic coefficient for conversion of ammonia into nitrite (1/d).

K_b: coefficient for coliform death as function of temperature, salinity, and predation (1/d).

K_{ca}: coefficient for the (flux of) growth of bottom algae ($gD/m^2\,d$).
K_{cf} (L): coefficient for the effect of solar light on phytoplankton growth (non-dimensional).
K_{cf} (N): coefficient for the effect of nutrients on phytoplankton growth (non-dimensional).
K_{cf} (T): coefficient for the effect of temperature on phytoplankton growth (1/d).
K_d: coefficient of effective deoxygenation in the river (1/d).
K_{di}: kinetic coefficient for the dissolution of detritus; normally in the range 0.3 to 0.7 (1/d).
K_{des}: kinetic coefficient for denitrification (1/d).
K_e: coefficient of solar light extinction (1/m).
K_{idegr}: coefficient of inhibition of deoxygenation by low DO concentration (L/mgO).
K_{ides}: coefficient of inhibition of denitrification (L/mgO).
K_{in}: kinetic coefficient for conversion of nitrite into nitrate (1/d).
K_{ini}: coefficient of inhibition of first stage nitrification by low DO concentration (L/mgO).
K_{ini}: coefficient of inhibition of first stage nitrification by low DO concentration (L/mgO).
K_{ma}: death rate of bottom algae (1/d).
K_{oa}: kinetic coefficient for conversion of organic nitrogen into ammonium (1/d).
K_{oi}: kinetic coefficient for conversion of organic phosphorus into orthophosphate (1/d).
Kp_{na}: coefficient for preference of bottom algae and phytoplankton for ammonium (mgN/L).
K_r: rate of decay of TC due to solar radiation (1/d).
K_{resf}: coefficient of inhibition of breathing due to low e DO concentration (L/mgO).
K_{rz}: kinetic coefficient for the respiration of phytoplankton; normally in the range 0.01 to 0.05 (1/d).
K_s: constant of half saturation (mg/L).
K_{Sct}: first order sedimentation coefficient (1/d).
Ks_{DBOc}: sedimentation coefficient for the BOD_c (1/d).
K_{Sff}: constant of half saturation for inorganic phosphorous; normally in the range 0.001 to 0.005 (mgP/L).
K_{Sg}: constant of half saturation for zooplankton grazing (mgA/L).
K_{Snf}: constant of half saturation for nitrogen; normally in the range 0.01 to 0.02 (mgN/L).
K_{Sfi}: constant of half saturation for phosphorus (mgP/L).
M_A: mass of bottom algae (mgD).
M_{CIT}: inorganic total carbon (mol).
M_D: mass of detritus (mgD).
M_{DBOc}: mass of BOD_c (mgO).
M_F: mass of phytoplankton (mgA).
M_{Fi}: mass of inorganic phosphorus (mgP).
M_{Fo}: mass of organic phosphorus (mgP).
M_{Na}: mass of ammonium nitrogen (mgN).
M_{Na}: mass of nitrite (mgN).
M_{Nn}: mass of nitrate (mgN).
M_{No}: mass of organic nitrogen (mgN).
M_{OD}: mass of dissolved oxygen (mgO).
M_{Si}: mass of inorganic solids (mg).
M_Z: mass of zooplankton (mgC).
n: effective daily duration of solar radiation (h).
N_m: maximum daily duration of solar radiation (h).
N: nutrient concentration (mg/L).
$N_{Al.}$: number of hydrogen gram equivalent ions (eqH^+).
N_{CT}: number of total coliforms (N_{org}).
pH_a: pH variation caused by autochtonous processes (non-dimensional).
$R[H^+]$,des: hydrogen gram equivalent ions per nitrogen mol consumed during denitrification ($eqH^+/molN$).
$R[H^+]$,na: hydrogen ions freed or consumed per mol of carbon when ammonium nitrogen is used as substratum ($eqH^+/molC$)
$R[H^+]$,nitri: gram equivalent hydrogen ions freed per mol of nitrified nitrogen ($eqH^+/molN$).
$R[H^+]$,nn: hydrogen ions freed or consumed per mol of carbon when nitrate is used as substratum ($eqH^+/molC$).
R_{ca}: carbon generated per unit of mass of a-chlorophyll (non-dimensional).
R_{cd}: mass of organic carbon liberated per mass of detritus dissolved in the water (non-dimensional).
R_{co}: mass of oxidized carbon per mass of consumed oxygen (non-dimensional).
R_{da}: stoichiometric ratio between detritus and a-chlorophyll used to express the mass of phytoplankton (non-dimensional).
$R_{mol,C}$: constant to transform mass of carbon into mols (molC/g).
$R_{mol,N}$: constant to transform mass of nitrogen into mols (molN/g).
R_{na}: mass of nitrogen liberated per mass of a-chlorophyll dissolved in the water (non-dimensional).
R_{nd}: mass of nitrogen liberated per mass of detritus dissolved in the water (non-dimensional).
R_{oc}: mass of consumed oxygen per mass of decomposed carbon (non-dimensional).
R_{ondes}: mass of non-used carbon per mass of denitrified nitrate (non-dimensional).
R_{oni}: mass of consumed oxygen per mass of oxidized ammonium (non-dimensional).
R_{onn}: mass of consumed oxygen per mass of oxidized nitrite (non-dimensional).
R_{pa}: coefficient for conversion of a-chlorophyll into phosphorous (non-dimensional).
R_{pd}: mass of organic phosphorous liberated per mass of detritus dissolved in the water (non-dimensional).
T : water temperature (^oC)
$TA_{Al.}$: rate of alkalinity increase caused by the aquatic vegetable community (eqH^+/d).

TA_{Fi}: rate of inorganic phosphorus assimilation by phytoplankton and bottom algae (mgP/d).
TA_{Na}: rate of ammonium assimilation by phytoplankton and bottom algae (mgN/d).
TA_{Nn}: rate of nitrate assimilation by phytoplankton and bottom algae (mgN/d).
T_{ar}: air temperature (^{o}C).
TC_A: rate of growth of bottom algae (mgD/d).
TC_F: rate of growth of bottom phytoplankton (mgA/d).
TC_Z: rate of growth of bottom zooplankton (mgC/d).
$TD_{Al.}$: rate of alkalinity decay caused by the aquatic vegetable community (eqH^+/d).
TD_{eCIT}: rate of increase of total inorganic carbon due to oxidation of organic carbon (mol/d).
TDe_{DBOc}: rate of degradation of organic carbon (mgO/d).
$TDes_{Al.}$: rate of increase of alkalinity due to denitrification (eqH^+/d).
$TDes_{DBOc}$: rate of decay of BOD_c due to denitrification (mgO/d).
$TDes_{Nn}$: rate of denitrification (mgN/d).
TD_{esOD}: rate of deoxygenation caused by the degradation of organic carbon (mgO/d).
TD_{Fo}: rate of decay of organic phosphorus (mgP/d).
TD_{iD}: rate of dissolution of detritus (mgD/d).
TD_{No} rate of decay of organic nitrogen (mgN/d).
TF_{CIT}: rate of decay of total inorganic carbon due to photosynthesis of phytoplankton and bottom algae (mol/d).
TF_{OD}: rate of increase dissolved oxygen due to photosynthesis (mgO/d).
TG_F: rate of zooplankton grazing (mgA/d).
TM_A: rate of death of bottom algae (mgD/d).
TM_{CT}: rate of death of total coliforms (N_{org}/d).
$TN_{iAl.}$: rate of decay of alkalinity due to nitrification (eqH^+/d).
TN_{Na}: rate of first stage nitrification (mgN/d).
TN_{Ni}**:** rate of second stage nitrification (mgN/d).
TN_{OD}: rate of DO loss due to nitrification (mgO/d).
TP_D:rate of production of detritus (mgD/d).
TP_{DBOc}: rate of production of BODc (mgO/d).
TP_{Fo}: rate of production of organic phosphorus (mgP/d).
TP_{Na}: rate of production of ammonium nitrogen (mgN/d).
TP_{No} rate of production of organic nitrogen (mgN/d).
TR_A: rate of respiration of bottom (mgD/d).
TR_{CIT}: rate of increase of inorganic carbon due to respiration of phytoplankton and bottom algae (mol/d).
TRe_{CO2}: rate of CO_2 transfer between water and atmosphere (mol/d).
TRe_{OD}: rate of surface superficial reoxygenation (gO/d).
TR_F: rate of phytoplankton respiration (mgA/d).
TR_{OD}: rate of decrease of DO due to respiration by phytoplankton and bottom algae (mgO/d).
TR_Z: rate of phytoplankton respiration (mgC/d).
TS_{CT}: rate of sedimentation of total coliforms (N_{org}/d).
TS_D: rate of sedimentation of detritus (mgD/d).
TS_{DBOc}: rate of sedimentation of BDOc (mgO/d).
TS_{si}: rate of sedimentation of inorganic solids (mg/L).
U_v: wind speed (m/s).
α: proportionality constant (≈ 1) (non-dimensional).
θA_m: coefficient of the effect of temperature on ammonification (non-dimensional).
θ_{CT}: coefficient of the effect of temperature on mortality (non-dimensional).
θD_i: coefficient of the effect of temperature on the dissolution of detritus (non-dimensional).
θF: coefficient of the effect of temperature on the growth of phytoplankton (non-dimensional).
θG_z: coefficient of the effect of temperature on zooplankton grazing (non-dimensional).
θH_{fo}: coefficient of the effect of temperature on organic phosphorus hydrolysis (non-dimensional).
θN: coefficient of the effect of temperature on nitrification (non-dimensional).
θR_e: coefficient of the effect of temperature on surface reoxygenation (non-dimensional).
θR_f: coefficient of the effect of temperature on phytoplankton respiration (non-dimensional).
θR_z: coefficient of the effect of temperature on zooplankton respiration (non-dimensional).
θS_{DBOc}: coefficient of the effect of temperature on sedimentation of BDO_c (non-dimensional).
μ_{ra}: rate of respiration of bottom algae (1/d).
μ_{rf}: kinetic coefficient for the respiration of phytoplankton (1/d).
σ: Stefan-Boltzmann constant (cal/cm^2 d K^4).
υ_d: apparent settling speed for detritus (m/d).
υ_{si}: apparent settling speed for inorganic solids (m/d).

REFERENCES

Brown L. C. & Barnwell T, O. (1987) The enhanced stream water quality models QUAL2E and QUAL2E-UNCAS: Documentation and user manual. *Environmental Research Laboratory, Office of Research and Development. U.S. EPA/600/3-87 /007.*

Chapra S. C. & Pelletier G. J. (2003) QUAL2K: A modeling framework for simulating river and stream water quality: documentation and user manual. *Civil and Environmental Engineering Dept., Tufts University, Medford.*

Chapra S. C., Pelletier G. J. & Tao H. (2007) QUAL2K: A modeling framework for simulating river and stream water quality: documentation and user manual. Version 2.07. *Civil and Environmental Engineering Dept., Tufts University, Medford.*

Di Toro, D. M. (2001) *Sediment Flux Modeling.* Wiley-Interscience, New York, USA.

Drolc, A. & Koncan, J. Z. (1996) Water quality modeling of the river sava, Slovenia. *Wat. Res.* **30**(11), 2587–2592.

Ghosh, N. C. & Mcbean, E. A. (1998) Water quality modeling of the Kali river, India. *Water, Air, and Soil Pollution.* **102**, 91-103.

Gonçalves, J. C. S. I., Sardinha, D. S. & Boesso, F. F. (2011) Modelo numérico para a simulação da qualidade da água no trecho urbano do rio Jaú, Município de Jaú-SP. *Revista de Estudos Ambientais.* **13**(2), 44-56.

Gonçalves, J. C. S. I., Sardinha, D. S., Souza, A. D. G., Dibiazi, A. L. B., Godoy, L. H. & Conceição, F. T. (2012) Avaliação espaço-temporal da qualidade da água e simulação de autodepuração na bacia hidrográfica do córrego São Simão-SP. *Revista Ambiente & Água*. 7(3), 141-154.

Liu, W.C., Liu, S. Y., Hsu, M. S. & Kuo, A. Y. (2005) Water quality modeling to determine minimum instream flow for fish survival in tidal rivers. *Journal of Environmental Management*. **52**, 55–66.

Park, S. S. & Lee, Y. S. A water quality modeling study of the Nakdong river, Korea. *Ecological Modelling*. **152**, 65-75.

Salvai, A. & Bezdan, A. (2008) Water quality model QUAL2K in TMDL development. Balwois Ohrid, Republic of Macedonia. **27**, 1-8.

Sardinha, D. S., Conceição, F. T., Souza, A. D. G., Silveira, A., de Júlio, M. & Gonçalves, J. C. S. I. (2008) Avaliação da qualidade da água e autodepuração do Ribeirão do Meio, Leme (SP). *Engenharia Sanitária e Ambiental*. **13**(3), 329-338.

Wang, H. Q. & Lacroix, M. (1997) Optimal weighting in the finite difference solution of the convection-dispersion equation. *Journal of Hydrology*. **200**, 228-242.

Zhang, R., Qian, X., Li, H., Yuan, X. & Ye, R. (2012) Selection of optimal river water quality improvement programs using Qual2K: A case study of Taihu Lake Basin, China. *Science of the Total Environment*. **431**, 278-285.